A spectroscopic search for non-radial pulsations in the δ Scuti star γ Bootis

R. Ventura,[1]★ G. Catanzaro,[1] J. Christensen-Dalsgaard,[2] M. P. Di Mauro[3] and L. Paternò[4]

[1]*INAF – Osservatorio Astrofisico di Catania, Via S. Sofia 78, 95123 Catania, Italy*
[2]*Institut for Fysik og Astronomi, Bygn. 1520, Aarhus Universitet, Ny Munkegade, DK-8000 Aarhus C, Denmark*
[3]*INAF–IASF, Istituto di Astrofisica Spaziale e Fisica Cosmica, Via del Fosso del Cavaliere 100, 00133 Roma, Italy*
[4]*Dipartimento di Fisica ed Astronomia, Università di Catania, Via S. Sofia 78, 95123 Catania, Italy*

ABSTRACT

High-resolution spectroscopic observations of the rapidly rotating δ Scuti star γ Bootis have been carried out in 2005, over six consecutive nights, in order to search for line-profile variability. Time-series, consisting of flux measurements at each wavelength bin across the Ti II 4571.917 Å line profile as a function of time, have been Fourier analysed.

The results confirm the early detection reported by Kennelly et al. of a dominant periodic component at frequency 21.28 cycles d^{-1} in the observer's frame, probably due to a high-azimuthal-order sectorial mode. Moreover, we found other periodicities at 5.06, 12.02 cycles d^{-1}, probably present but not secure, and at 11.70 and 18.09 cycles d^{-1}, uncertain. The latter frequency, if present, should be identifiable as another high-azimuthal-order sectorial mode and the three additional terms as low-l modes as proved by the analysis of the first three moments of the line. Owing to the short time baseline and the one-site temporal sampling we consider our results only preliminary but encouraging for a more extensive multisite campaign.

A refinement of the atmospheric physical parameters of the star has been obtained from our spectroscopic data and adopted for preliminary computations of evolutionary models of γ Bootis.

Key words: stars: individual: γ Bootis – stars: individual: HD127762 – stars: oscillations – δ Scuti.

1 INTRODUCTION

δ Scuti stars are typically Population I, A and F main-sequence or slightly post-main-sequence variables of mass $M = 1.4$–$3.0\,M_\odot$, either in a stage of H-core or H-shell burning, with projected rotational velocity $v \sin i$ in the range of 10–$200\,km\,s^{-1}$. They are located in the lower part of the classical instability strip where the κ mechanism is expected to drive radial and non-radial p modes, modes with mixed p and g character and possibly also g modes. Many of these variables are observed to be low-amplitude, multimode pulsators with power spectra sufficiently rich to allow an asteroseismological investigation.

Photometry of δ Scuti stars has allowed to identify low-degree ($l \leqslant 3$), low-order ($n \leqslant 7$) p modes (see Garrido 2000; Poretti 2000, for exhaustive reviews), while additional information came from spectroscopic studies which have confirmed the presence of high-degree non-radial modes with l up to 20 (Mantegazza 2000) in moderate or fast rotators.

In these stars pulsation modes of high degree manifest themselves as cyclical line-profile variability characterized by the appearance of weak (less than 1 per cent of continuum) absorption moving bumps travelling across the rotationally broadened profiles from side to side. Rapid rotation enhances the visibility of high-degree modes because it allows to spatially resolve the wave pattern of the photospheric velocity fields across the stellar disc, leading to a one-to-one correspondence between wavelength in the broadened line profile and position on the stellar surface (the so-called Doppler imaging). Adjacent velocity fields of opposite sign, travelling around the star due to rotation, produce opposite Doppler shifts, effectively causing a redistribution of the flux across the rotationally broadened line profile and then the appearance of characteristic absorption moving distortions (Vogt & Penrod 1983). The apparent period of variations is the time for the pattern to repeat itself and it is related to both the phase velocity of the wave and the rotational velocity of the star.

★E-mail: rve@oact.inaf.it

Moving bumps in δ Scuti stars were first observed by Yang & Walker (1986) and Walker, Yang & Fahlman (1987). From then on, the number of rapidly rotating δ Scuti stars showing high-degree modes has increased progressively thanks both to the improvements in spectroscopic techniques and theoretical developments which have triggered an extensive monitoring of stars suspected to be non-radial pulsators. To date, 16 δ Scuti high-degree pulsators (see Mantegazza 2000; Balona et al. 2001; Koen et al. 2002) have been studied in detail for line-profile variability.

Among these stars, γ Bootis (HD127762, A7III) is a bright ($V = 3$), rapidly rotating δ Scuti star that belongs to a transition group located between the main-sequence variables and the Cepheids. Photometric variations with a period of $P = 0.25$ d have been reported by Auvergne, Le Contel & Baglin (1979). This star is among the few δ Scuti stars with a period longer than 0.20 d (see Rodríguez, López-González & López de Coca 2000). Line-profile variations in the spectra of the star were detected for the first time by Kennelly et al. (1992). The authors collected a total of 29 spectrograms, at a time cadence of about 10 min, in two different periods, three months apart, covering a total observing time of about 5 h. They analysed the data by sampling at 1.5 Å intervals the intensity of the residuals built by subtracting the mean profile from each profile in the series, and then computing the amplitude spectra in the Fourier domain. A period of variation in moving distortions of 0.047 ± 0.002 d was found and interpreted as a high-degree ($|m| \simeq 10$) non-radial mode with a period of 0.073 d in the corotating frame. The series were not long enough to cover a full cycle of the known photometric period reported by Auvergne et al. (1979) so that Kennelly et al. (1992) obtained only a rough confirmation of it. Since then, to the best of our knowledge, no further and more accurate investigations on pulsations of the star have been reported in literature.

In this paper we present the results of new careful spectroscopic observations of γ Boo performed on a baseline of six nights at the INAF – Catania Astrophysical Observatory. In Section 2 we describe the acquisition and reduction of the data. In Section 3 we discuss the procedures adopted to determine the atmospheric parameters of the star, necessary to construct realistic models of the star, and those to analyse the line-profile variability and present the results. Finally, in Section 4 we discuss the implications of our finding and draw some conclusion.

2 OBSERVATIONS AND DATA REDUCTION

Time-resolved spectroscopy of γ Boo was carried out during six consecutive nights, from 2005 June 21 to 26, by means of the RE-OSC echelle spectrograph operating with the 91-cm telescope of the INAF – Catania Astrophysical Observatory.

The spectrograph is fibre-linked to the telescope through an ultraviolet–near-infrared type fibre of 100 μm core diameter. It is designed to work both at high resolution, in cross-dispersion mode, and at low resolution, in single-dispersion mode. The observations were performed in the cross-dispersion configuration making use of both gratings: the 300 grooves mm^{-1} echellette grating, blazed at $4°.3$ whose maximum efficiency is about 80 per cent at the blaze wavelength 5000 Å, and the echelle grating with 79 grooves mm^{-1} blazed at $63°.443$. Spectra were acquired through a thinned, back-illuminated CCD with 1024×1024 pixels of 24 μm size, whose typical readout noise is about 6.5 e^{-} and photon gain 2.5 ph ADU^{-1}. The resulting spectral range was approximately from 4300 to 6700 Å (19 orders).

Table 1. Observation log of γ Bootis spectroscopy.

Heliocentric Julian Date (245 0000+)	δT (h)	Number of spectra
3543.319 58	6.28	67
3544.371 64	3.77	43
3545.316 69	6.44	71
3546.334 66	5.56	59
3547.319 94	5.83	65
3548.316 79	5.62	62

A total of 367 spectrograms, covering 33.5 h of observation (see Table 1), were obtained. The spectrograms were extracted from the CCD images and calibrated in wavelengths by using the NOAO/IRAF package. In the spectral region covered by our observations, owing to the relatively high value of the projected rotational velocity, only the Ti II 4571.917 Å line was found completely free from blends of adjacent features, thus suitable to allow a good normalization to the stellar continuum and a study of the line-profile variability. In the spectral region of the selected line the resulting reciprocal dispersion was 0.12 pixels mm^{-1} with an effective resolving power of $R \approx 16\,000$, as deduced from the emission lines of the Th–Ar calibration lamp. The integration time for each exposure was set to 5 min with a resulting signal-to-noise ratio (S/N) up to 200. This exposure time was optimized in such a way as to avoid phase-smearing effects. Finally, the spectra have been corrected in order to remove the observer's velocity variation due to the Earth's revolution and rotation, and the continuum in the proximity of the line was defined by a linear least-squares fit of two spectral windows selected on both red and blue sides of the line.

3 DATA PROCESSING

3.1 Determination of the atmospheric parameters and abundance analysis

The atmospheric structure of γ Bootis has been studied by several authors in the last decades (see Table 2). Auvergne et al. (1979) found an effective temperature $T_{eff} = 8000$ K, a surface gravity $\log g = 3.8$ and a projected rotational velocity $v \sin i = 145$ $km\,s^{-1}$, values adopted later by Kennelly et al. (1992).

More recently, Erspamer & North (2003), based on Elodie spectrograms, derived for the star a slightly lower effective temperature

Table 2. Parameters of γ Bootis.

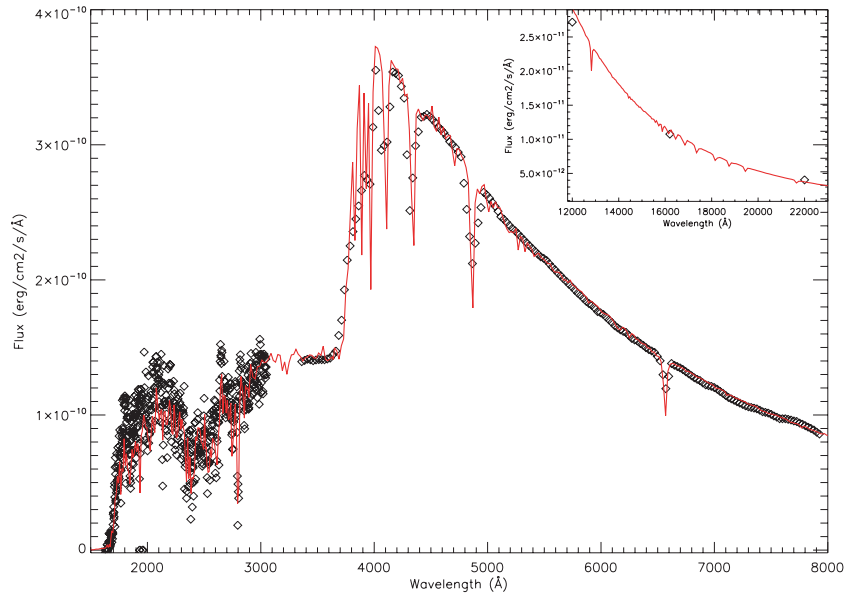|	
Parallax	38.29 ± 0.73 mas (*Hipparcos* Main Catalogue)
V	3.04
$B - V$	0.191
$U - B$	0.120
Spectral type	A7 III
$v \sin i$	145 $km\,s^{-1}$ (Auvergne et al. 1979)
	123 $km\,s^{-1}$ (Erspamer & North 2003)
	128 $km\,s^{-1}$ (Royer et al. 2002)
	115 $km\,s^{-1}$ (Abt & Morrell 1995)
T_{eff}	8000 K (Auvergne et al. 1979)
	7585 K (Erspamer & North 2003)
M_V	0.93
Photometric frequency	0.25 d (Auvergne et al. 1979)
Spectroscopic frequency	0.0047 d (Kennelly et al. 1992)

Figure 1. Observed spectral energy distribution (SED) built from various literature sources as described in the text. Thick line represents theoretical SED computed by ATLAS9 code for $T_{\rm eff} = 7600$ K and $\log g = 3.70$.

$T_{\rm eff} = 7585$ K and values of surface gravity $\log g = 3.75$, micro-turbulent velocity $\xi = 3.1$ km s^{-1} and $v \sin i = 123$ km s^{-1}. The last value is also in good agreement with that reported by Royer et al. (2002), based on Aurelie spectrograms, who found $v \sin i = 128$ km s^{-1}, while Abt & Morrell (1995) derived from CCD Coudé spectra a slightly lower value of 115 km s^{-1}.

To determine effective temperature and surface gravity for our star, we proceeded in two consecutive steps: (i) we derived atmospheric parameters by matching the observed flux distribution obtained by joining various data sources collected from the literature and (ii) we refined the values found in the previous step by modelling the observed H_β line profile. In step (i), the observed flux (see Fig. 1) has been built using the following data.

(i) *IUE* spectra processed with the NEWSIPS reduction method taken from INES Final Archive data. The data consist of two high-dispersion spectra (SWP44484RL and LWP25820RL) that we co-added manually for obtaining a unique spectrum covering the 1150–3350 Å interval;

(ii) spectrophotometry in the range 3200–7900 Å taken from Burnashev (1985);

(iii) *UBV* magnitudes from Johnson & Morgan (1953);

(iv) *JHK* magnitudes from Two Micron All Sky Survey (2MASS) (Skrutskie et al. 2006).

The resulting spectrum has been dereddened following the procedure by Cardelli, Clayton & Mathis (1989) and then compared to a grid of theoretical fluxes computed by means of ATLAS9 code (Kurucz 1993) with convection turned on ($l/H = 1.25$). The colour excess, $E(B - V)$, needed by the dereddening procedure has been derived from $E(b - y) = 0.01$ (Gray, Napier & Winkler 2001) using the relation $E(b - y) = 0.74 E(B - V)$ (Crawford 1975). The starting values of $T_{\rm eff}$ and $\log g$ have been obtained from the Strömgren photometry of γ Bootis (Hauck & Mermilliod 1998) according to the grid of Moon & Dworetsky (1985). The photometric colours have been dereddened with the Moon (1985) algorithm. From this calculation we found $T_{\rm eff} = 7600$ K and $\log g = 3.70$.

In step (ii), we compared the observed profile of the H_β line with the synthetic one, minimizing the differences between them by using the χ^2-criterion to evaluate the goodness of fit. Errors were estimated as the variation in the parameters which increases the χ^2 by a unit. The observed spectrum we use from here on is the average of all the collected data. The final S/N ranges between 230 and 360.

By adopting the iterative procedure described in Catanzaro, Leone & Dall (2004), which takes into account also metal abundances, and by using as input data the values derived in step (i), we obtained the final values: $T_{\rm eff} = 7600 \pm 150$ K and $\log g = 3.75 \pm 0.05$, which are in good agreement with those obtained by Erspamer & North (2003). With these values we then computed the synthetic profile shown in Fig. 2 by means of the SYNTHE (Kurucz & Avrett 1981) spectral synthesis code for a local thermodynamic equilibrium
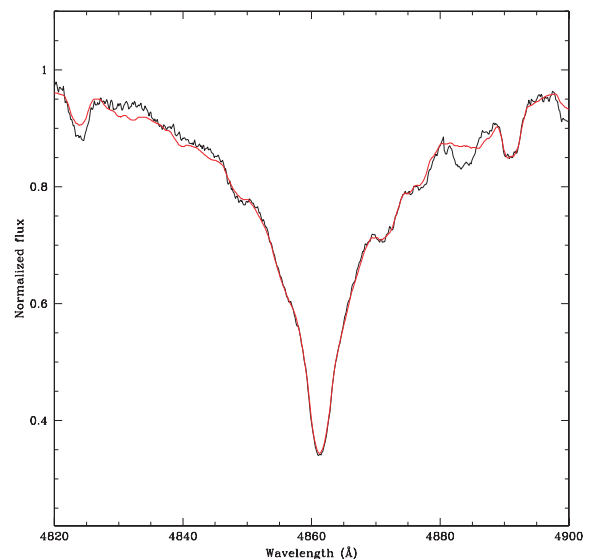

Figure 2. Comparison between the observed and computed H_β line profile.

Table 3. Basic parameters of γ Bootis as derived by the present analysis.

$v \sin i$	$115 \pm 2 \text{ km s}^{-1}$
T_{eff}	$7600 \pm 150 \text{ K}$
$\log g$	3.75 ± 0.05

Table 4. Abundances of chemical elements derived for γ Bootis with respect to their abundances in the solar atmosphere (Grevesse & Sauval 1998) expressed as $[X/H] = \log(N_X/N_H)_\star - \log(N_X/N_H)_\odot$. For comparison we report the abundances determined for γ Bootis by Erspamer & North (2003) (third column).

Element	This study	E&N (2003)
Na	0.45	0.25
Mg	−0.05	0.16
Si	−0.01	0.06
Ca	−0.01	0.04
Sc	−0.04	0.35
Ti	0.25	0.01
Cr	−0.17	−0.14
Mn	−0.01	−0.20
Fe	−0.08	−0.20
Ni	−0.22	−0.22
Ba	−0.10	0.15

(LTE) atmospheric model with solar metallicity (opacity distribution function = [0.0]) calculated by using the ATLAS9 (Kurucz 1993) stellar atmosphere program.

The projected rotational velocity has been previously estimated by a non-linear least-squares fit of a rotationally broadened Gaussian profile to the average line profile of the Ti II λ4571.917 Å. The derived value of $115 \pm 2 \text{ km s}^{-1}$ is in excellent agreement with those previously derived by Royer et al. (2002) and Abt & Morrell (1995). The calculated values of $T_{\text{eff}}, \log g, v \sin i$ are listed in Table 3.

In order to calculate the atmospheric element abundances of γ Bootis we computed the synthetic spectrum of the star in the whole observed spectral region by assuming the above derived values of $T_{\text{eff}}, \log g, v \sin i$ and the microturbulent velocity ξ by Erspamer & North (2003). We used ATLAS9 (Kurucz 1993) in order to compute the LTE atmospheric model and SYNTHE (Kurucz & Avrett 1981) program in order to identify the observed spectral lines and derive its chemical abundances. The LINUX version of both codes are those implemented by Sbordone et al. (2004). The values of the oscillator strengths $\log gf$ for each spectral line are those published by Kurucz & Bell (1995) and the subsequent upgrading by Castelli & Hubrig (2004). The derived abundances in terms of solar abundances $[X/H] = \log(N_X/N_H)_\star - \log(N_X/N_H)_\odot$, assuming the solar values by Grevesse & Sauval (1998), are reported in Table 4. For comparison we report also the abundances derived by Erspamer & North (2003). The deduced uncertainties are typically of the order of 0.1 dex.

As a general result we obtained for γ Bootis chemical abundances quite close to the solar values at least up to Ni ($Z = 28$), a common feature in the abundance pattern of many δ Scuti stars (Yushchenko et al. 2005). Erspamer & North (2003) stated that in the range of T_{eff} and $\log g$ they have considered, errors on abundances are typically

less than 0.15 dex. These results allow us to conclude that abundances derived in our study, and reported in Table 4, are compatible with their values, the discrepancies being always consistent with experimental errors.

3.2 Line-profile variations

As mentioned in Section 2, owing to the relatively high rotational velocity of the star, the only spectral line completely free from line-blend contamination, and therefore suitable for a study of line-profile variability, was the Ti II 4571.917 Å line.

The Fourier analysis of the Ti II 4571.917 Å line-profile variations was performed by adopting the so-called pixel-by-pixel method (Mantegazza 2000), based on the fact that the flux measured at each wavelength bin across a line profile fluctuates with the same period as a wave propagating in the photosphere of the star. Therefore from the whole set of 367 residual spectrograms we extracted 40 time-series (as many as the pixels sampling the Ti II 4571.917 Å line profile) consisting of the measured fluxes at each wavelength across the line profile as a function of time. The Fourier transform of the resulting time-strings was performed by adopting the generalized version of the least-squares multiple sinusoid fit with known constituents (Mantegazza & Poretti 1995), originally developed by Vanicek (1971). A 'global' least-squares spectrum, which contains the contribution to the variability coming – on the whole – from the full set of the time-series (i.e. from the whole line profile), is computed iteratively every time a 'known periodic constituent' has already been detected and a new $n + 1$ periodic term is searched for. A simultaneous least-squares fit of $n + 1$ sinusoids is performed exploring the entire domain of trial frequencies ν_i, and a power spectrum is generated by defining the global reduction factor

$$\text{RF}_i = 1 - \sum_{j,k} w_k^2 [p_{i,j}(t_k) - P(j, t_k)]^2 / \sigma_n,$$

where $p_{i,j}(t_k)$ is the multisinusoidal function adopted to fit the jth time-series, $P(j, t_k)$, sampled at time t_k, σ_n is the global residual variance after the fit of the line-profile variations with the n known constituents and w_k are the normalized weights derived from the S/N of the spectrograms. The frequency ν_i corresponding to the highest value of RF is then selected as the $(n + 1)$th known constituent and the procedure is iterated again until when no dominant peaks appear in the last power spectrum. The technique does not rely on pre-whitening of the data, and amplitudes and phases of the known constituents are recomputed, together with their formal errors, each time a new periodic component has been detected. A more detailed description of this approach can be found in Mantegazza & Poretti (1999) and Mantegazza (2000).

On adopting the procedure described above, we computed the least-squares global power spectrum by scanning the whole frequency range from 0 up to the Nyquist frequency, which is around 140 cycles d^{-1}, with a spacing of 0.04 cycles d^{-1}. However, all the power spectra reported here have been truncated at 40 cycles d^{-1} since all the significant power appears at frequency well below 30 cycles d^{-1}. The total length of the data set is such that the half-width at half-maximum of the main power peak in the window function is 0.095 cycles d^{-1}. Fig. 3 reports both the least-squares pixel-by-pixel power spectra without known constituents, which describes the evolution of the variability across the line profile, and the corresponding global spectrum. It is evident in both of them the presence of a prominent periodicity centred at 21.28 cycles d^{-1}, also reported by Kennelly et al. (1992) in their analysis of line-profile
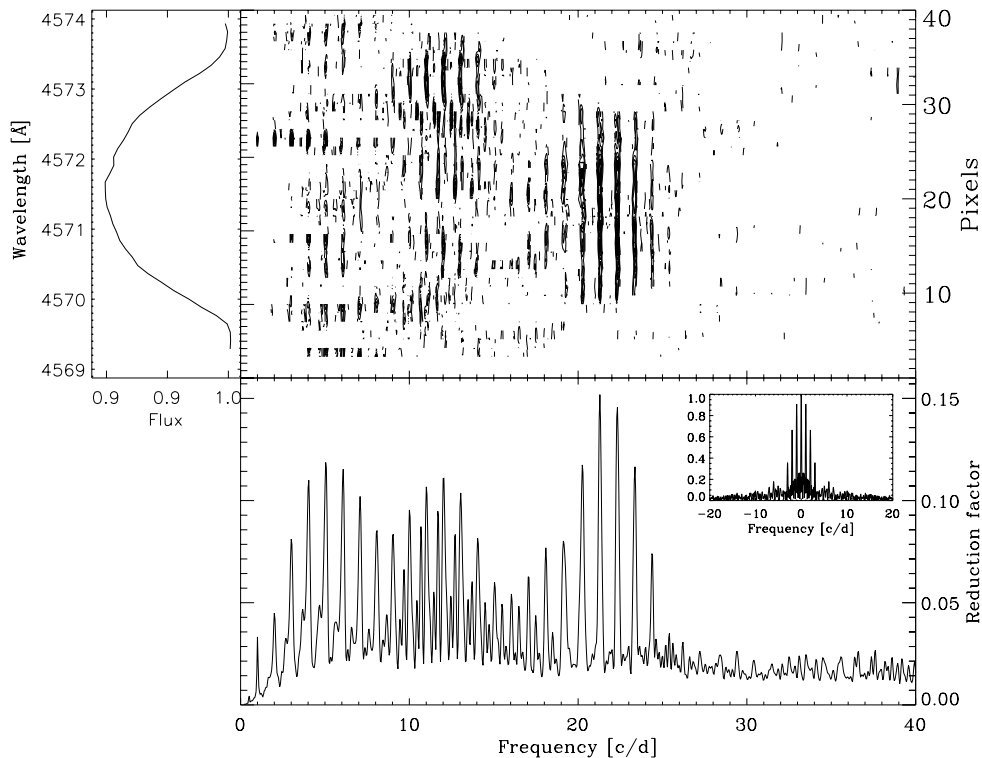
Figure 3. Pixel-by-pixel least-squares analysis of the variability of the Ti II 4571.917 Å line profile. Top left-hand panel: average profile. Top right-hand panel: pixel-by-pixel least-squares power spectra without known constituents, describing the evolution of the Ti II 4571.917 Å line-profile variability as a function of the wavelength bin across the line profile. Bottom panel: global least-squares power spectrum without known constituents. The inset shows the amplitude spectrum of the window function.

variability. A very sharp thread of power corresponding to this frequency extends all over the core of the line profile and beyond, and covers about the 55 per cent of the whole profile. Quite strong daily aliases of the central peak, produced by the limited single-site temporal sampling (see the spectral window in the inset of the figure) distributed over six consecutive nights, flank the true frequency. Significant concentrations of power are also present around 12 and 5 cycles d^{-1}. Their distribution across the line profile is discontinuous, but patches of power corresponding to these periodicities are present all across the line profile and extend even towards the line wings.

The extraction of frequencies from the iterative least-squares fitting procedure was performed paying particular attention to the possibility that the strong daily aliases produced by the single-site sampling of our data, and the limited frequency resolution resulting from the observing baseline, can lead to a wrong identification of the true frequencies. We computed spectra with an increasing number of known constituents and with various possible combinations of frequencies considering not only the highest peaks (which indeed could be the aliases of the true frequencies) but also contiguous features at ±1 cycles d^{-1}, following the procedure suggested by Mantegazza, Poretti & Zerbi (1995). The least-squares fitting procedure described above allowed us to extract iteratively the following independent frequencies, reported in order of detection: 21.28, 5.06, 12.02, 18.09 and 11.70 cycles d^{-1}. It is worth noting that the second frequency extracted is very close to the frequency of the mode photometrically detected by Auvergne et al. (1979).

Fig. 4 shows the pixel-by-pixel power spectra and the corresponding global least-squares spectrum obtained at the end of the iterative procedure when all the known constituents have been removed from the data. Most part of the signal disappeared, but weak residual peaks at low frequencies are still present. A further iterative step of computation, however, did not allow us to identify firmly any additional periodic component. This is probably due to the limited data window of our data set. More observations on a longer baseline might contribute to clarify this point.

In order to investigate further the reliability of the five-frequency least-squares fit solution, we divided the data set in two subsets three nights long (see Table 1), and analysed them separately, with the aim of verifying if the same frequencies occur in both subsets. The power spectra without known constituents computed for the two subsets are shown in Fig. 5; they appear quite noisy, as expected, but the same three power concentrations detected in the whole data set spectrum are still present in both subsets. The frequency resolutions of the two subsets are 0.22 and 0.23 cycles d^{-1}, respectively, to be compared with the 0.095 cycles d^{-1} for the complete data set.

Though the separation of data into two subsets is in principle essential for determining the reliability of the identified frequencies, since in our case the data sampling in each subset is poor only the gross features can be taken into consideration. From an analysis of the power spectra of the two subsets it appears that the main frequency at 21.28 cycles d^{-1} is present in both the subsets (with the aliases at the frequencies of 20.21 and 22.30 cycles d^{-1}), as well as the one at 5.06 cycles d^{-1} (with the aliases at the frequencies of 4.06 and 7.08 cycles d^{-1}), and probably the one at 12.02 cycles d^{-1} (but not present in the first subset); the frequencies at 11.70 and 18.09 cycles d^{-1} appear only when the whole set of data is considered. From this analysis we can conclude that: (i) the main frequency at 21.28 cycles d^{-1} is almost certainly present, but from the present data alone it cannot be ruled out that the true frequency might
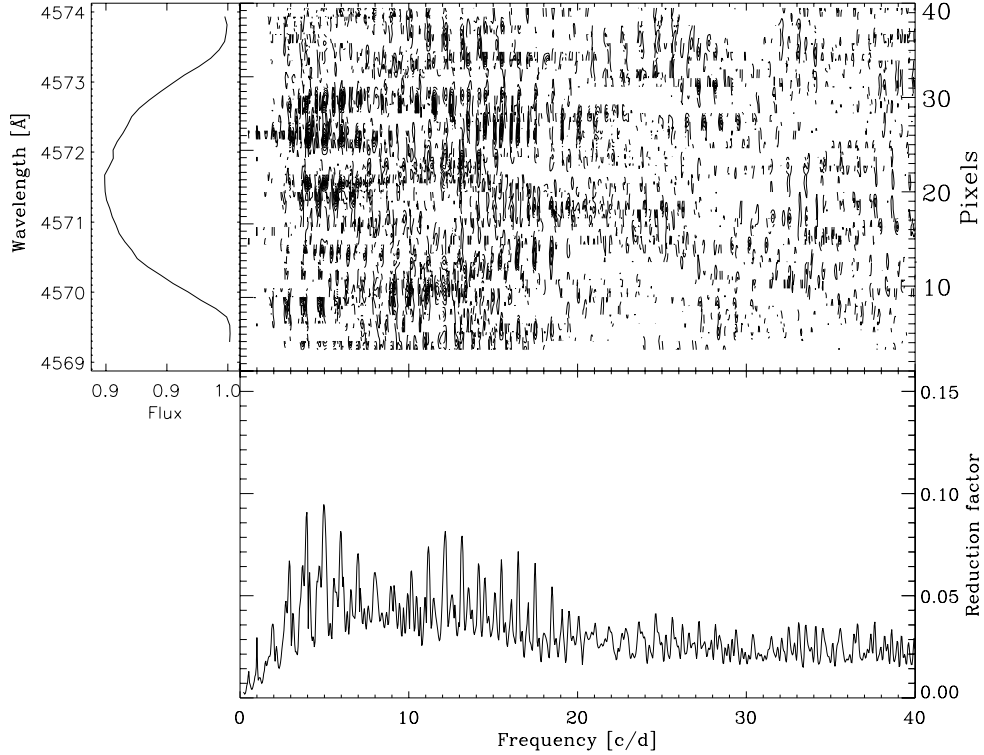
Figure 4. Pixel-by-pixel least-squares power spectra and global least-squares power spectrum obtained after all the known constituents have been removed from the data. In the upper panel the noise appears to be increased with respect to Fig. 3 because each panel has been normalized to its maximum value.
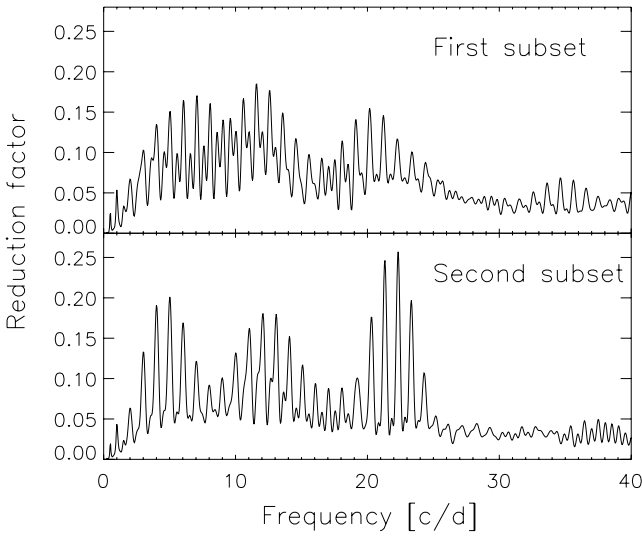

Figure 5. Global least-squares power spectra without known constituents for the first (upper panel) and second subset (lower panel).

actually be 20.28 or 22.28 cycles d^{-1}; (ii) the frequency at 5.06 cycles d^{-1} is probably present, but the true frequency might well be 4.06 or 6.06 cycles d^{-1}; (iii) the frequency at 12.02 cycles d^{-1} might be present, but certainly not secure; (iv) the frequencies at 11.70 and 18.09 cycles d^{-1} are uncertain.

Although the spectral resolution of our data does not allow any rigorous mode identification, some useful clues for a very broad characterization of the detected frequencies can be derived from the analysis of the phase behaviour across the line profile for each so-

lution of the final multiple-sinusoidal fit. Actually it is well known that the phase diagrams give a full and independent representation of the line-profile variability caused by each individual pulsation mode and are considered useful tools for characterizing the detected variability (see Telting & Schrijvers 1997). Only the phase diagrams referring to the components at 21.28, 18.09 and 11.70 cycles d^{-1} show a clear signature (see Fig. 6), while those of the components at 5.06 and 12.02 cycles d^{-1} are quite uncertain and
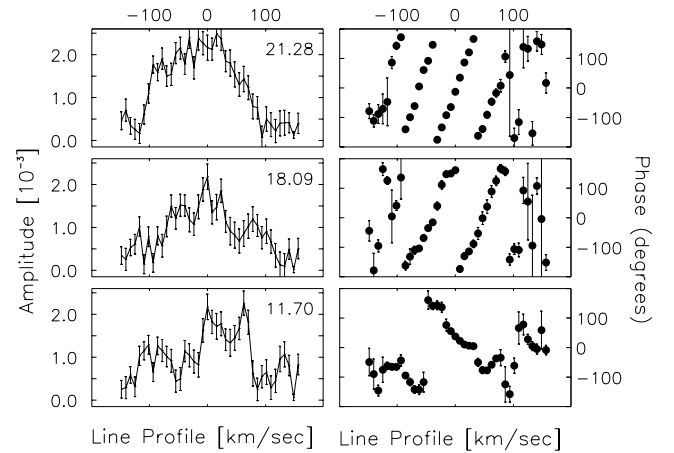

Figure 6. Behaviour of amplitudes (left-hand panels) and the phases (right-hand panels) across the profile of the Ti II 4571.917 Å line of the periodic components 21.28, 18.09 and 11.70 cycles d^{-1} detected in the line-profile variation analysis. Wavelengths along the line profile have been converted into Doppler velocities relative to the line centre. The bars are the formal errors as derived by the global least-squares simultaneous fit. The frequency in cycles d^{-1} of each component is reported at the top of each panel.

do not supply any useful discriminant. In Fig. 6 the wavelengths of the line profile have been converted into Doppler velocities assuming zero velocity at the centre of the line. The error bars correspond to the formal errors derived from the least-squares fit. The phase diagrams of both the main component at frequency 21.28 cycles d^{-1} and the component at 18.09 cycles d^{-1} show the typical behaviour of high-azimuthal-order retrograde modes, i.e. their phase increases in the same direction of the stellar rotation, namely with the wavelength. According to the commonly adopted expression exp[i($m\phi + 2\pi\nu t$)], which describes the time and longitude dependence of a pulsation at frequency ν, it follows that both the cited modes are characterized by positive m-values. The number of phase lines in both the diagrams indicates that the azimuthal order should be quite high for both terms. In order to get a quantitative estimate of the m-value for both modes we measured the shift in velocity δv between the two central phase lines measured at the centre of the line profile and deduced the separation $\delta\phi$ in longitude between the two equiphasic points from the relation $\delta\phi = 2 \arcsin(\delta v/(2v_e))$, where v_e is the equatorial rotation velocity, assuming for simplicity an equator-on view of the star ($i = 90°$). Since $|m| = 360/\delta\phi$, we obtained $|m| = 11.47 \pm 0.7$ for the component at 21.28 cycles d^{-1} and $|m| = 9.16 \pm 0.7$ for the mode at 18.09 cycles d^{-1}. The derived $|m|$-value for the component at 21.28 cycles d^{-1} is in excellent agreement with that reported by Kennelly et al. (1992). If we assume again an equator-on geometry, the probability to be detected is higher for sectorial modes ($l = |m|$) since they are mainly focused at the equator of the star. In this hypothesis the two components at 21.28 and 18.09 cycles d^{-1} should be $l = m = 11$ and $l = m = 9$ retrograde modes, respectively. Other interpretations are obviously possible since it has been demonstrated that tesseral modes with $l - |m|$ small, observed at an inclination angle of about 50°, might produce similar moving patterns as sectorial modes observed equator-on (i.e. Schrijvers et al. 1997). The presence of retrograde modes in δ Scuti stars, though much less frequent than prograde ones, is not uncommon (Mantegazza 2000; Mantegazza, Poretti & Zerbi 2001; Kennelly et al. 1998). The phase diagram relevant to the term at frequency 11.70 cycles d^{-1} appears compatible with a low-degree prograde $m < 0$) mode.

In order to catch additional information on the nature of the detected periodicities, we computed the equivalent width and the first three moments (which describe the centre-of-mass velocity of the line, the linewidth and the line skewness, respectively) of the Ti II 4571.917 Å line profile, as a function of time, following the prescriptions given by Balona et al. (1996) and Schrijvers et al. (1997). Since the moments are quantities integrated over the whole line profile they are expected to be essentially sensitive to low-degree modes ($l \leqslant 4$). We then analysed the resulting time-series by adopting the software package for Fourier analysis and least-squares multiple-sinusoids fitting, PERIOD04 (Lenz & Breger 2005) to search for periodicities. Useful results have been obtained only from the zero, second and third moments (see Fig. 7), while the periodogram of the first moment is quite noisy.

The periodogram of the equivalent width of the line shows a concentration of power around the frequency 6.05 cycles d^{-1} which could be the 1 cycle d^{-1} alias of the frequency 5.06 cycles d^{-1}, detected also in the line-profile variations and probably corresponding to the dominant photometric mode. The second-order moment variability is characterized by two significant components at 10.69 and 3.01 cycles d^{-1}, respectively. The former of the two frequencies, which appears to be slightly favoured by the analysis compared with the adjacent peak at 11.69 cycles d^{-1}, could actually be the one-day
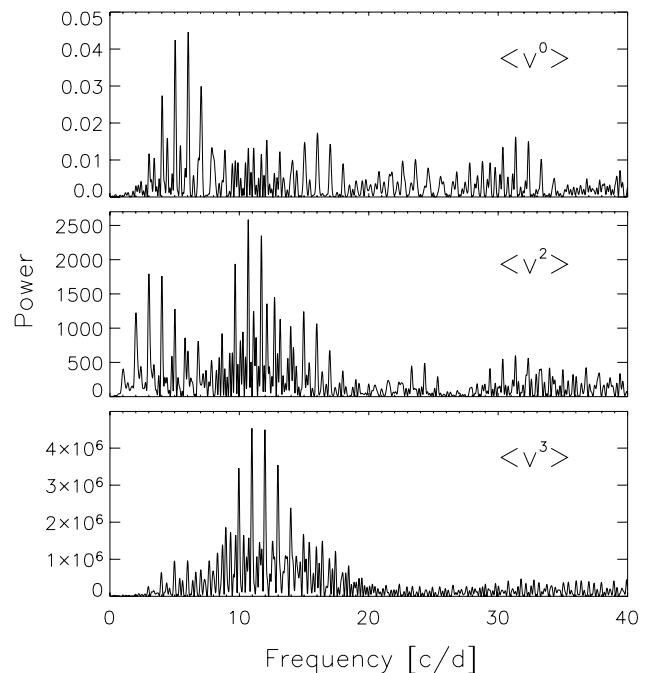

Figure 7. Power spectra of the moments of zero (upper panel), second (middle panel) and third order (bottom panel) obtained by the software package PERIOD04.

Table 5. Observed oscillation frequencies and the present tentative at mode identification (see Section 3).

Frequency (cycles d^{-1})	l	m
21.28	$\geqslant 10$	10, 11, 12
18.09	$\geqslant 8$	8, 9, 10
12.02	?	?
11.70	$\leqslant 4$	$-4 \leqslant m \leqslant -1$
5.06	$\leqslant 4$	$-4 \leqslant m \leqslant 4$

alias of the term at 11.70 cycles d^{-1}, also detected in the line-profile variation analysis. The periodogram of the third moment shows a clump of power in the frequency range 5–20 cycles d^{-1} with a significant feature present at 11.69 cycles d^{-1}. Other significant terms peak at 10.97, 17.43 and 5.08 cycles d^{-1}. Once again the last value appears to be consistent with the result of the pixel-by-pixel line-profile variation analysis which gives 5.06 cycles d^{-1}. The presence of the components at 5.06 and 11.70 cycles d^{-1} in the variability of the first three moments might support their identification in terms of low-l ($\leqslant 4$) modes. Moreover, the simultaneous presence of the term at 11.69 cycles d^{-1} in the power spectra of both the second and third moments might allow us to rule out the possibility that the mode might be axisymmetric ($m = 0$) (Balona 1986). As may be expected for high-degree pulsation modes, in the Fourier analysis of the moments there is no trace of the components at either 21.28 or 18.09 cycles d^{-1}, detected in the line-profile variation analysis and interpreted as high-azimuthal-order retrograde modes.

A summary of the results obtained is given in Table 5 in which oscillation frequencies, tentative harmonic degree l, and azimuthal order m of the detected modes are listed.

4 CONCLUSION

The new spectroscopic data of γ Bootis presented here confirm the early detection of the main pulsation component at 21.28 cycles d^{-1}

found by Kennelly et al. (1992). Additional frequencies were detected at 18.09, 12.02, 11.70 and 5.06 cycles d^{-1}. The analysis of the phase diagrams relevant to each component supplied useful hints for characterizing the detected variability. In particular, the two terms at 21.28 and 18.09 cycles d^{-1} appear to be high-azimuthal-order retrograde modes. In the hypothesis of an equator-on view of the star we suggest a tentative interpretation in terms of sectorial modes for both of them with $m = l = 11$ and $m = l = 9$, respectively. The identification proposed for the main component is in general good agreement with the conclusion of the work by Kennelly et al. (1992). Moreover, the component at 11.70 cycles d^{-1} is probably a low-l prograde mode. The frequency analysis of the first three moments seems to confirm this interpretation and supplies a constraint on m, suggesting that the mode is not axisymmetric. The phase diagrams of the two additional terms at 5.06 and 12.02 cycles d^{-1} are quite uncertain and do not supply any useful discriminant.

The results obtained strongly encourage the planning of new observations with a higher S/N and spectral resolution in order to get an unambiguous discrimination among the possible identifications of the modes by performing a direct fitting of the line-profile variations to pulsational models. Simultaneous photometric observations could also allow to model at the same time the flux variations in the line profiles.

Preliminary calculations of evolutionary models of γ Bootis constrained within the uncertainties of the present parameter determinations indicate that this star has a mass of about $2\,M_\odot$ and an age of about 0.9 Gyr, an immediate post-main-sequence subgiant star.

REFERENCES

Abt H. A., Morrell N. I., 1995, ApJS, 99, 135
Auvergne M., Le Contel J. M., Baglin A., 1979, A&A, 76, 15
Balona L. A., 1986, MNRAS, 219, 111
Balona L. A. et al., 1996, MNRAS, 281, 1315
Balona L. A. et al., 2001, MNRAS, 321, 239
Burnashev N. I., 1985, Abastumanskaya Astrofiz. Obs. Bull., 59, 83
Cardelli J. A., Clayton G. C., Mathis J. S., 1989, ApJ, 345, 245
Castelli F., Hubrig S., 2004, A&A, 425, 263
Catanzaro G., Leone F., Dall T. H., 2004, A&A, 425, 641
Crawford D. L., 1975, AJ, 80, 955
Erspamer D., North P., 2003, A&A, 398, 1121
Garrido R., 2000, in Breger M., Montgomery M. H., eds, ASP Conf. Ser. Vol. 210, Delta Scuti and Related Stars. Astron. Soc. Pac., San Francisco, p. 67
Gray R. O., Napier M. G., Winkler L. I., 2001, AJ, 121, 2148
Grevesse N., Sauval A. J., 1998, Space Sci. Rev., 85, 161
Hauck B., Mermilliod M., 1998, A&AS, 129, 431
Johnson H. L., Morgan W. W., 1952, ApJ, 117, 313
Kennelly E. J. et al., 1998, ApJ, 495, 440
Kennelly E. J., Yang S., Walker G. A. H., Hubeny I., 1992, PASP, 104, 15
Koen C., Balona L., van Wyk F., Marange F., Paunzen E., 2002, MNRAS, 330, 567
Kurucz R. L., 1993, in Dworetsky M. M., Castelli F., Faraggiana R., eds, IAU Colloq. 138, ASP Conf. Ser. Vol. 44, Peculiar versus Normal Phenomena in A-type and Related Stars. Astron. Soc. Pac., San Francisco, p. 87
Kurucz R. L., Avrett E. H., 1981, SAO Special Report, 391
Kurucz R. L., Bell B., 1995, Kurucz CD-ROM No. 23. Smithsonian Astrophysical Observatory, Cambridge, MA
Lenz P., Breger M., 2005, Communications in Asteroseismology, 146, 53
Mantegazza L., 2000, in Breger M., Montgomery M. H., eds, ASP Conf. Ser. Vol. 210, Delta Scuti and Related Stars. Astron. Soc. Pac., San Francisco, p. 138
Mantegazza L., Poretti E., 1995, ASP Conf. Ser. Vol. 83, Insights into the Pulsational Behaviour of δ SCT Stars. Astron. Soc. Pac., San Francisco, p. 337
Mantegazza L., Poretti E., 1999, A&A, 348, 139
Mantegazza L., Poretti E., Zerbi F. M., 1995, A&A, 299, 427
Mantegazza L., Poretti E., Zerbi F. M., 2001, A&A, 366, 547
Moon T. T., 1985, Communications from the University of London Observatory, p. 78
Moon T. T., Dworetsky M. M., 1985, MNRAS, 217, 305
Poretti E., 2000, in Breger M., Montgomery M. H., eds, ASP Conf. Ser. Vol. 210, Delta Scuti and Related Stars. Astron. Soc. Pac., San Francisco, p. 45
Rodríguez E., López-González M. J., López de Coca P., 2000, A&AS, 144, 469
Royer F., Grenier S., Baylac M.-O., Gòmez A. E., Zorec J., 2002, A&A, 393, 897
Sbordone L., Bonifacio P., Castelli F., Kurucz R., 2004, Mem. Soc. Astron. Ital. Suppl., 5, 93
Schrijvers C., Telting J. H., Aerts C., Ruymaekers E., Henrichs H. F., 1997, A&AS, 121, 343
Skrutskie M. F. et al., 2006, AJ, 131, 1163
Telting J. H., Schrijvers C., 1997, A&A, 317, 723
Vanicek P., 1971, Ap&SS, 12, 10
Vogt S. S., Penrod G. D., 1983, ApJ, 275, 661
Walker G. A. H., Yang S., Fahlman G. G., 1987, ApJ, 320, L139
Yang S., Walker G. A. H., 1986, PASP, 98, 1156
Yushchenko A., Gopka V., Chulhee K., Musaev F., Kang Y. W., Kovtyukh V., Soubiran C., 2005, MNRAS, 359, 865

This paper has been typeset from a TeX/LaTeX file prepared by the author.